

New Methods for Interpretation of Magnetic Gradient Tensor Data

David A. Clark

CSIRO Materials Science and Engineering
PO Box 218
Lindfield, NSW 2070
Australia
David.Clark@csiro.au

SUMMARY

Recent technological advances suggest that we are on the threshold of a new era in applied magnetic surveys, where acquisition of magnetic gradient tensor data will become routine. In the meantime, modern ultrahigh resolution conventional magnetic data can be used, with certain important caveats, to calculate gradient tensor elements from total magnetic intensity (TMI) or TMI gradient surveys. Until the present, not a great deal of attention has been paid to processing and interpretation of gradient tensor data. New methods for inverting gradient tensor surveys to obtain source parameters have been developed for a number of elementary, but useful, models. These include point pole, line of poles, point dipole (sphere), line of dipoles (horizontal cylinder), thin and thick dipping sheets, sloping step and contact models. A key simplification is the use of eigenvalues and associated eigenvectors of the tensor. The scaled source strength, calculated from the eigenvalues, is a particularly useful rotational invariant that peaks directly over compact sources, 2D sources and contacts, independent of magnetisation direction. New algorithms for uniquely determining the location and magnetic moment of a dipole source from a few irregularly located measurements or single profiles have been developed. Besides the geological applications, these algorithms are readily applicable to the detection, location and classification (DLC) of magnetic objects, such as naval mines, UXO, shipwrecks, archaeological artefacts and buried drums. As an example, some of these new methods are applied to analysis of the magnetic signature of the Mount Leyshon gold-mineralised system, Queensland.

Key words: Magnetic gradient tensor, eigenvalues, eigenvectors, dipole localisation, Mount Leyshon

INTRODUCTION

A number of authors (e.g. Pedersen and Rasmussen, 1990; Christensen and Rajagopalan, 2000; Schmidt and Clark, 2006; Foss, 2006) have discussed theoretical advantages of magnetic gradient tensor measurements over conventional magnetic surveys. Over the past decade there has been growing interest in developing new high sensitivity full tensor magnetic gradiometer systems. Slow but steady progress has been made with SQUID magnetometer/gradiometer systems, both low T liquid He-cooled (e.g. Clem *et al.*, 1997) and high T liquid nitrogen-cooled (Clem *et al.*, 2001; Young *et al.*, 2010), particularly for

military applications such as naval mine detection and unexploded ordnance detection. Over the last decade the first practical low T SQUID-based system for geophysical gradient tensor surveys has been developed by the Jena (Germany) group (Stolz *et al.*, 1999, 2006a,b; Chwala *et al.*, 2001). The intrinsic noise of the LTS planar gradiometers developed by this group is 0.2 pT/m (integrated between 0.01 Hz and 10 Hz). Noise spectral density of the full tensor gradiometer system in motion is about 1-10 pT/m/ $\sqrt{\text{Hz}}$ over a frequency range of 0.1-2 Hz in a bird towed beneath a helicopter and approximately ten times higher for installation on a fixed wing aircraft.

The discovery of high T (liquid nitrogen temperatures and above) superconducting materials in the late 1980s has created opportunities for cheaper, smaller devices that can be readily transported and refilled, but retain very high sensitivities. Liquid nitrogen cooled SQUIDs and gradiometers are very sensitive, with noise levels that are about an order of magnitude higher than those of low T SQUIDs. Clark *et al.* (1998) suggested the use of combined vector field and gradient tensor measurements, using high T superconducting devices, for separating contributions of induced and remanent magnetisation to magnetic anomalies and for inferring source properties, such as total magnetisation direction, remanence direction and Koenigsberger ratio.

Humphrey *et al.* (2005) have demonstrated a high T SQUID-based gradiometer, designed for use on a mobile platform, with correction for common mode signals provided by vector sensors, combined with active compensation of ambient fields. This system attained white noise levels, above ~ 3 Hz, of 1 pT/m/ $\sqrt{\text{Hz}}$ while undergoing roll/pitch/yaw motions of $\pm 5^\circ$.

The availability of flexible high T superconducting tapes has allowed development of an intrinsic axial gradiometer (Tilbrook, 2004). Substantial improvements in common mode rejection of ambient magnetic fields and reduction in noise are achieved by spinning the gradiometer and detecting the second harmonic of the rotation frequency (Leslie *et al.*, 2005; Tilbrook *et al.*, 2006). This concept was the basis for a prototype manually rotated full tensor gradiometer for ground measurements, which was successfully demonstrated over the Tallawang deposit (Schmidt *et al.*, 2004). Further development has seen a successful helicopter-borne trial of a spinning gradiometer system (Leslie *et al.*, 2007), which measured gradient tensor components with sensitivities down to 50 pT/m at a sampling rate of 10 Hz. A target intrinsic sensitivity of 10 pT/m is believed to be achievable with this system.

Although the inherent sensitivity of fluxgate magnetometers is far inferior to that of superconducting devices, a practical fluxgate-based tensor gradiometer, capable of mapping anomalies greater than about 10 nT/m in mobile operation, has

been developed (Bracken and Brown, 2006). Wiegert et al. (2007) describe a multiple tensor gradiometer system, comprising an array of eight triaxial low noise fluxgate magnetometers, that has a sensitivity of about 0.25 nT/m in hand-carried mobile operation.

Other proposed technologies include a stiff metallic string carrying an AC current tuned to the second eigenmode of mechanical vibration, which is sensitive to an off-diagonal term of the gradient tensor (Veryaskin, 2001; McRae et al., 2004; Sunderland et al., 2009). Although this technique only measures a single tensor component, the full gradient tensor could in principle be obtained from an array of differently oriented string sensors. The noise spectrum of this instrument is very flat over the frequency range of interest, with the $1/f$ corner at ~ 2.5 mHz. The current white noise floor, measured in the geomagnetic field, obtained with this method is 0.4 nT/m/ $\sqrt{\text{Hz}}$ from 0.01-0.625 Hz (Sunderland et al., 2009), which corresponds to a rms noise level of 0.3 nT/m over this bandwidth. The target sensitivity for static measurements is 0.01 nT/m.

The brief review above suggests that we are on the threshold of a new era in applied magnetic surveys, where acquisition of magnetic gradient tensor data will become routine.

Efficient use of the extra information provided by gradient tensor surveys will require creative new processing and interpretation. Contributions to this effort include Pedersen and Rasmussen (1990), Schmidt *et al.* (2004), Schmidt (2006), Fitzgerald and Holstein (2006), Heath (2007), Clark *et al.* (2009), Fitzgerald *et al.*, (2009, 2010), Beiki *et al.* (2011) and Holstein *et al.* (2011). In this paper, I outline several new approaches to interpretation of gradient tensor data and present preliminary analysis of the well-known Mount Leyshon anomaly in the Charters Towers area, Queensland.

New methods developed for analysis of magnetic gradient tensor data can also be applied to high quality conventional TMI surveys that have been processed using Fourier filtering techniques to calculate magnetic vector and tensor components. This approach is, in fact, the only practical way at present to analyse vector component data, as measurements of vector components are seriously afflicted by motion noise, which is not as serious a problem for gradient components.

While it should be stressed that direct measurement of the gradient tensor will provide superior results, useful gradient tensor data can be obtained by Fourier processing of TMI surveys, provided a number of caveats are addressed. These include: effective removal of regional trends and careful windowing of survey areas, to minimise artefacts such as Gibbs phenomenon “ringing” and spectral leakage; a density of sampling (particularly across lines) that is sufficient to effectively eliminate aliasing of high frequencies in the measured fields; reliable interpolation algorithms to provide accurate (not just “pretty”) gridded TMI data for Fourier domain calculation of gradient tensor elements; and accurate reduction of TMI data to a common level before Fourier processing, using equivalent source methods or otherwise, which is a very challenging requirement in areas of rugged topography.

It can be shown by an analysis similar to that of Reid (1980) that the grid spacing of TMI measurements can be no more

than about half the depth to the sources, for accurate calculation of tensor components, with negligible aliasing.

Careful regularisation of the filtering process is essential when the geomagnetic inclination is low, because calculation of vector components from TMI surveys becomes unstable close to the geomagnetic equator (Blakely, 1996, p.342-343). This is true *a fortiori* for calculation of gradient tensor elements. Furthermore, if intense anomalies are present, measured TMI data must be corrected to a true potential field, as outlined by Schmidt and Clark (2006) and Fleury and Munsch (2010).

THE MAGNETIC GRADIENT TENSOR

The magnetic gradient tensor \mathbf{B} is defined as the vector gradient of the magnetic field vector \mathbf{b} :

$$\mathbf{B} = \nabla \mathbf{b}. \quad (1)$$

For magnetostatic fields in the absence of conduction currents,

$$\nabla \times \mathbf{b} = 0, \quad (2)$$

which implies that \mathbf{b} can be expressed as the gradient of a scalar potential:

$$\mathbf{b} = [b_x, b_y, b_z]^T - \nabla \Omega = - \left[\frac{\partial \Omega}{\partial x}, \frac{\partial \Omega}{\partial y}, \frac{\partial \Omega}{\partial z} \right]^T, \quad (3)$$

where Ω is the magnetic scalar potential.

With respect to Cartesian axes \mathbf{B} has nine components, B_{ij} ($i, j = x, y, z$), which may be displayed as a matrix:

$$\mathbf{B} = \begin{bmatrix} B_{xx} & B_{xy} & B_{xz} \\ B_{yx} & B_{yy} & B_{yz} \\ B_{zx} & B_{zy} & B_{zz} \end{bmatrix} = \begin{bmatrix} \frac{\partial b_x}{\partial x} & \frac{\partial b_y}{\partial x} & \frac{\partial b_z}{\partial x} \\ \frac{\partial b_x}{\partial y} & \frac{\partial b_y}{\partial y} & \frac{\partial b_z}{\partial y} \\ \frac{\partial b_x}{\partial z} & \frac{\partial b_y}{\partial z} & \frac{\partial b_z}{\partial z} \end{bmatrix}. \quad (4)$$

In a source free region Ω and its derivatives of all orders are continuously differentiable functions. From (3) and (4), this implies that the tensor is symmetric:

$$B_{ij} = B_{ji}, \forall i, j, \quad (5)$$

a conclusion which also follows directly from (2).

Furthermore, since

$$\nabla \cdot \mathbf{b} = \frac{\partial b_x}{\partial x} + \frac{\partial b_y}{\partial y} + \frac{\partial b_z}{\partial z} = 0, \quad (6)$$

it follows that the tensor is traceless:

$$B_{xx} + B_{yy} + B_{zz} = 0. \quad (7)$$

The symmetry and tracelessness of the tensor imply that, of the nine tensor components, only five are independent. Equations (3) and (6) imply that Ω obeys Laplace's equation, i.e. it is a potential field that can be continued analytically in source-free space. It is easily shown that derivatives of Ω of all orders are also potential fields, so vector and tensor components measured over a plane can be continued to different levels and vertical derivatives can be calculated using standard techniques (see Blakely, 1996, Chapter 12).

EIGENVECTOR ANALYSIS OF THE TENSOR

Eigenvalues and eigenvectors are discussed in many textbooks on linear algebra, e.g. Anton and Rorres (2000). Eigenvectors of \mathbf{B} satisfy by definition the relationship $\mathbf{B}\mathbf{v} = \lambda\mathbf{v}$, for some scalar λ , which is the eigenvalue corresponding to \mathbf{v} . The eigenvalues are found by solving the characteristic equation $\det(\mathbf{B} - \lambda\mathbf{I})$. Expanding the determinant gives a cubic equation in λ :

$$\lambda^3 + I_1\lambda - I_2 = 0, \quad (8)$$

where

$$I_1 = B_{yy}B_{zz} + B_{xx}B_{yy} + B_{zz}B_{xx} - B_{xy}^2 - B_{xz}^2 - B_{yz}^2, \quad (9)$$

$$I_2 = \det(\mathbf{B}) = B_{xx}B_{yy}B_{zz} - B_{xx}B_{yz}^2 - B_{zz}B_{xy}^2 - B_{yy}B_{xz}^2 + 2B_{xy}B_{xz}B_{yz}. \quad (10)$$

The coefficient of λ^2 in the cubic equation for λ vanishes because the tensor is traceless. It can be shown that the quantities I_1 and I_2 are unchanged by rotation of the coordinate axes, i.e. they are rotational invariants of the tensor. They have the neat property that they can be simply expressed directly in terms of the tensor components with respect to any Cartesian reference frame. Pedersen and Rasmussen (1990) discuss applications of these standard invariants to interpretation of potential field surveys.

Each distinct root of the cubic equation defines a distinct eigenvalue of the tensor. For each eigenvalue λ_i , the corresponding eigenvectors can be found as non-zero vectors \mathbf{v}_i that satisfy $\mathbf{B}\mathbf{v}_i = \lambda_i\mathbf{v}_i$, which can then be normalised to define unit eigenvectors.

Since \mathbf{B} is a symmetric real 3×3 matrix, all its eigenvalues are real, eigenvectors corresponding to distinct eigenvalues are orthogonal, and an orthonormal set of three eigenvectors can always be found, including the case of degenerate (i.e. two equal) eigenvalues (Anton and Rorres, 2000, p.357-358). The matrix \mathbf{R} that has these three unit eigenvectors as its columns is a rotation matrix that diagonalises \mathbf{B} (*ibid*, p.349). That is, with respect to Cartesian axes along the eigenvectors the rotated tensor \mathbf{B}' , is given by

$$\mathbf{B}' = \mathbf{R}\mathbf{B}\mathbf{R}^{-1} = \mathbf{R}\mathbf{B}\mathbf{R}^T = \begin{bmatrix} \lambda_1 & 0 & 0 \\ 0 & \lambda_2 & 0 \\ 0 & 0 & \lambda_3 \end{bmatrix}. \quad (11)$$

It is easily shown that the eigenvalues of \mathbf{B} are rotational invariants of the tensor. Evidently, any combination of the eigenvalues is also a rotational invariant. Conversely, any rotational invariant $f(B_{xx}, B_{yy}, B_{zz}, B_{xy}, B_{yz}, B_{xz})$ can be expressed as a combination of eigenvalues since, by definition, this function of the tensor elements is unchanged by rotation into the principal axis frame, where it is equal to $f(\lambda_1, 0, 0, \lambda_2, 0, 0, \lambda_3)$.

A particularly useful rotational invariant is the scaled source strength, which can be expressed as the following combination of eigenvalues:

$$\mu = \sqrt{-I_1 - 2\lambda_2^2} = \sqrt{-\lambda_2^2 - \lambda_1\lambda_3}. \quad (12)$$

For 2D sources the scaled source strength is equal to the total gradient (analytic signal amplitude) of the vertical field component or, equivalently, the total gradient of the strike-perpendicular horizontal component. It is proportional to, but always larger than, the total gradient of the TMI, particularly for meridionally striking structures at low latitudes. In the 2D case, therefore, μ has the desirable property that it is independent of magnetisation direction.

For several useful 2D and 3D models (e.g. the point pole, line of poles, point dipole, line of dipoles (horizontal cylinder), thin dipping sheet, and contact models), μ peaks directly above the source. For these models the scaled source strength is a homogeneous function with a simple $1/r^n$ fall-off, suitable for Euler deconvolution, and the width of the μ anomaly is simply related to the source depth.

A general symmetric second order tensor has three independent rotational invariants (scalars), e.g. the three eigenvalues, or various combinations of eigenvalues such as their sum (the trace of the tensor), their product (the determinant I_2) and the sum of pairwise products (the invariant I_1). If, like the magnetic gradient tensor, the tensor is traceless, then any two eigenvalues determine the third. In this case there can only be two independent rotational invariants of the tensor.

Eigenvector analysis of the gradient tensor has a number of important applications. For example, Beiki et al. (2011) have recently demonstrated the utility of eigenvector analysis of the pseudogravity gradient tensor, which can be calculated from TMI surveys if the magnetisation direction is known, or can be assumed.

For a number of important magnetic model types, eigenvector analysis of the gradient tensor yields some simple direct solutions for model parameters. For point pole and line of pole models the major eigenvectors (associated with the largest magnitude eigenvalue) point directly toward the source, allowing its location to be obtained by triangulation. A gradient tensor anomaly for which, at all points within the main anomaly, two eigenvalues are approximately equal and the third is opposite in sign and double the magnitude, is diagnostic of a pole-like source. The magnetic anomaly vector \mathbf{b} is radial, pointing directly away from the pole of strength p if p is positive and directly towards the pole if $p < 0$. Thus

$$\mathbf{b} = \frac{Cp}{r^2} \hat{\mathbf{r}}, \quad (13)$$

where $\hat{\mathbf{r}}$ is the unit outward radial vector from the source and C is a constant that depends on the units used. For pole strength in Am, distances in metres, magnetisations in A/m, and fields in nT, $C = 100 \text{ nTmA}^{-1}$. The magnitude of the magnetic anomaly vector, $|\mathbf{b}| = Cp/r^2$, is a maximum directly above the pole. However, the total magnetic intensity (TMI) anomaly does not peak over the pole, except when the geomagnetic field is vertical. The eigenvalues in non-increasing order of absolute value are:

$$\lambda_1 = -C \frac{2p}{r^3}, \lambda_2 = \lambda_3 = C \frac{p}{r^3}. \quad (14)$$

At every observation point the eigenvalues are proportional to the vertical component of the anomalous field:

$$\lambda_1 = \frac{2B_z}{h}, \lambda_2 = \lambda_3 = -\frac{B_z}{h}, \quad (15)$$

so the ratio of the vertical component over an eigenvalue provides an estimate of the depth of the source. For a point pole, the scaled source strength is simply equal to the absolute value of the degenerate eigenvalues ($\mu = |\lambda_2|$).

For 2D sources the intermediate eigenvalue (with the smallest absolute value) is close to zero and the corresponding eigenvector indicates the strike. The scaled source strength is simply equal to the absolute value of the nonzero eigenvalues for 2D sources.

ANALYSIS OF DIPOLE SOURCES

The point dipole model is applicable to any sufficiently compact magnetised body. Outside a spherical surface that completely encloses an arbitrary magnetised body, the field can be expressed as a sum of multipole contributions, with a $1/r^3$ fall-off for the dipole term, $1/r^4$ fall-off for the quadrupole, $1/r^5$ fall-off for the octupole term, and so on. Thus for any compact body with a non-zero dipole moment the far field is always dominated by the dipole term. More specifically, the external fields and gradients due to a uniformly magnetised sphere are identical to that of a point dipole, because the quadrupole and all higher multipole moments vanish identically.

As well as its importance in a geological context, the point dipole model is widely used in other applications. These include detection, location and classification of magnetic objects, such as naval mines, unexploded ordnance, shipwrecks, and archaeological artefacts.

A number of methods have been proposed for locating dipole targets from magnetic gradient tensor data (e.g. Wynn et al. 1975; Wilson, 1985; Wynn, 1995, 1997). Methods based on point-by-point analysis of the eigenvectors of the tensor tend to be adversely affected by noise in individual measurements of the gradient tensor elements. Furthermore, there is an inherent four-fold ambiguity in obtaining solutions for dipole location and orientation of its moment from point-by-point analysis of gradient tensors (Wynn et al., 1975; Wilson, 1985), which must be resolved by comparing solutions from different sensor locations, rejecting those that are not consistent (the so-called ‘ghost’ solutions) and retaining the solutions that exhibit the best clustering. Existing methods of dipole tracking are also not robust to the contamination of the

measured signal by variable background gradients, interfering anomalies, instrument drift or departures of the target from a pure dipole source.

Nara et al. (2006) have presented a neat solution to the single point dipole location problem that uses measurements of the anomalous field vector and gradient tensor, if accurate values of both are available. Along a fixed direction, the field vector \mathbf{b} is equal to a geometric factor, depending only on the magnitude and orientation of the magnetic moment \mathbf{m} , divided by r^3 . Using this fact it can be shown that the displacement vector from the dipole to the measurement point *independent* of the orientation of \mathbf{m} , is given by:

$$\mathbf{r} = -3\mathbf{B}^{-1}\mathbf{b}, \quad (16)$$

even though each tensor element and vector component on the RHS of this expression depends on \mathbf{m} . Equation (16) is applicable provided $\det\mathbf{B}$ is nonzero, so that the matrix representation of the tensor is invertible. The special case where \mathbf{B} is singular occurs when the measurement point lies within the plane orthogonal to the dipole axis, and is easily treatable separately.

Although Nara et al. (2006) did not treat this aspect, once the location of the dipole is known, determination of the moment becomes a straight-forward linear inversion problem. If the anomalous field vector \mathbf{b} is known to sufficient accuracy, the moment $\mathbf{m} = m(L, M, N) = (m_x, m_y, m_z)$ can be calculated as (Lima et al., 2006):

$$\mathbf{m} = \frac{r^3}{C} \left[\begin{array}{c} 3\mathbf{b} \cdot \mathbf{r} \\ 2r^2 \mathbf{r} - \mathbf{b} \end{array} \right]. \quad (17)$$

Similarly, given the location $\mathbf{r} = r(n_1, n_2, n_3)$ of the dipole, the expressions for its gradient tensor elements can be rewritten as

$$\boldsymbol{\rho} = \left[\begin{array}{c} r^4 B_{xx} \\ r^4 B_{xy} \\ r^4 B_{xz} \\ r^4 B_{yy} \\ r^4 B_{yz} \end{array} \right] = \mathbf{N} \left[\begin{array}{c} m_x \\ m_y \\ m_z \end{array} \right], \quad (18)$$

where

$$\mathbf{N} = 3C \left[\begin{array}{ccc} 3n_1 - 5n_1^3 & n_2 - 5n_1^2 n_2 & n_3 - 5n_1^2 n_3 \\ n_2 - 5n_1^2 n_2 & n_1 - 5n_1 n_2^2 & -5n_1 n_2 n_3 \\ n_3 - 5n_1^2 n_3 & -5n_1 n_2 n_3 & n_1 - 5n_1 n_3^2 \\ n_1 - 5n_1 n_2^2 & 3n_2 - 5n_2^3 & n_3 - 5n_2^2 n_3 \\ -5n_1 n_2 n_3 & n_3 - 5n_2^2 n_3 & n_2 - 5n_2 n_3^2 \end{array} \right]. \quad (19)$$

The LHS of (19) and the matrix \mathbf{N} contain only known quantities. This overdetermined matrix equation can be solved in a least squares sense for the components of the moment in terms of these known parameters:

$$\mathbf{m} = \mathbf{N}^+ \boldsymbol{\rho} = (\mathbf{N}^T \mathbf{N})^{-1} \mathbf{N}^T \boldsymbol{\rho}, \quad (20)$$

where \mathbf{N}^+ denotes the pseudoinverse of \mathbf{N} .

The method of Nara *et al.* (2006) can be extended to uniquely determining the dipole location and moment vector from the gradient tensor and the second order gradient (which is a third rank tensor B_{ijk}) at a measurement point. Along a fixed direction, B_{ij} is equal to a geometric factor, depending only on the magnitude and orientation of \mathbf{m} , divided by r^4 . From this it is easily shown that:

$$(\mathbf{r} \cdot \nabla) B_{ij} = -4 B_{ij}, \quad (21)$$

which gives an invertible linear relationship between \mathbf{r} , and first and second order gradient tensor elements. The system of linear equations is overdetermined, so only a subset of the second order gradients is needed to obtain a unique location. For example, if the gradient tensor is measured along a profile segment, parallel to the x axis, the dipole location can be calculated directly from the tensor and its along-profile derivative, which can be calculated by numerical differentiation:

$$\mathbf{r} = \begin{bmatrix} x - x_0 \\ y - y_0 \\ -h \end{bmatrix} = -4 \begin{bmatrix} \frac{\partial B_{xx}}{\partial x} & \frac{\partial B_{xy}}{\partial x} & \frac{\partial B_{xz}}{\partial x} \\ \frac{\partial B_{xy}}{\partial x} & \frac{\partial B_{yy}}{\partial x} & \frac{\partial B_{yz}}{\partial x} \\ \frac{\partial B_{xz}}{\partial x} & \frac{\partial B_{yz}}{\partial x} & \frac{\partial B_{zz}}{\partial x} \end{bmatrix}^{-1} \begin{bmatrix} B_{xx} \\ B_{xy} \\ B_{xz} \end{bmatrix}. \quad (22)$$

The moment of the dipole can then be determined from \mathbf{r} and the gradient tensor as shown above. Thus the dipole location and moment can be found from the first and second order gradient tensors at a single point. This result was inferred empirically by Wynn (1995) and later proved explicitly by him (Wynn, 1997). However that proof does not provide a method for determining the location and moment vector of the dipole. Wynn's (1995) method for inverting the gradient tensor and its along-profile gradients is quite complicated and involves a computationally intensive numerical search algorithm.

The second method presented here analyses data collected along a profile that passes near a dipole target. Unlike most other gradient tensor inversion techniques, this method can correct for contamination of the dipole signature by geological gradients or instrumental drifts, for example. Full details are given in Clark (2008).

Wilson (1985) showed that the scaled moment μ of a dipole, which is a particularly useful rotational invariant because it is independent of magnetic moment orientation and always peaks at the closest point of approach, can be calculated directly from the eigenvalues λ_i of the tensor. A sequence of calculated scaled moments along a profile can be deconvolved and interference terms estimated and removed, but in practice it is easier and to process a related quantity, which yields more robust solutions. Define another invariant that is independent of the dipole orientation by $\nu = \sqrt{(\mu/3)} = \{[\sqrt{(-\lambda_2^2 - \lambda_1 \lambda_3)}/3]\}^{1/2}$, where λ_2 is the eigenvalue with the smallest absolute value. For a pure dipole signature ν is proportional to $\sqrt{m/r^2}$. Then at any point around an isolated dipole source ν can be estimated

from the measured eigenvalues. In the presence of background gradients or interference from neighbouring bodies, at successive points $x = x_i$ ($i = 1, 2, \dots, n$) along a straight and level path, defined by $y - y_0 = Y$, ν determined from the measured data can be modelled as:

$$\nu_i = \frac{\sqrt{Cm}}{(x_i - x_0)^2 + S^2} + a + bx_i + cx_i^2, \quad (23)$$

where $S = \sqrt{Y^2 + h^2}$ is the slant distance from the point of closest approach to the dipole, $x = x_0$ is the point of closest approach, h is the depth of the dipole, a is the base level, and b, c are linear and quadratic terms that represent interference from other anomalies. The deconvolution problem is to solve for the unknown parameters x_0, S, m, a, b, c . This is equivalent to conventional Werner deconvolution (e.g. Ku and Sharp, 1983) of the TMI anomaly of a thin sheet.

Once the origin of x and slant distance are determined and the scaled moment, μ_i , and distance to source, r_i , at successive points are known, the measured gradient tensor elements can be modelled by:

$$B_{xx}^{(i)} = -\frac{\mu_i}{r_i^3} \left[2Lx_i^3 + 4MSx_i^2 - 3LS^2x_i - MS^3 \right] + a_{xx} + b_{xx}x_i + c_{xx}x_i^2, \quad (24)$$

with similar terms for the other four independent tensor elements, where the distances along the profile, x_i , are now with respect to an origin at the point of closest approach, $M = MY - Nh$ is the direction cosine of the slant component of magnetization and a quadratic interference term is assumed for each component. The deconvolution problem is to solve for the unknown parameters L, M, N , (direction cosines of the magnetisation direction) Y, h and the interference terms a_{ij}, b_{ij}, c_{ij} . This is carried out in a similar way to the deconvolution of the invariant ν (Clark, 2010). At this stage it is recommended to remove the interference terms from the measured tensor elements and recalculate the eigenvalues and ν . Using the new estimates of x_0, S, m the deconvolution of the tensor elements can be repeated. The process is generally rapidly convergent, the revised interference terms become small and the source parameters become more precisely determined.

ANALYSIS OF THE MOUNT LEYSHON ANOMALY

The mineralised system associated with the former Mount Leyshon gold mine in Queensland produces a prominent TMI magnetic low due to strong remanent magnetisation, acquired in the Early Permian, of reverse polarity (Sexton *et al.*, 1995; Clark and Lackie, 2003). Sexton *et al.* (1995) showed that the magnetic anomaly is substantially attributable to early potassic (biotite-magnetite) alteration of Palaeozoic host rocks (dolerite and metasilstones) and associated quartz-magnetite veins. This alteration zone is largely peripheral to the mineralised breccia and porphyry complex, so that the anomaly is slightly offset to the SW of the mine. The hydrothermal magnetite grains are generally quite fine-grained, with a substantial proportion within the pseudosingle domain size range, and retain a stable remanence that is directed south and steeply down.

Magnetic vector components and gradient tensor elements were derived from high quality publicly available TMI data by Fourier filtering. Figure 1 shows images over the Mount Leyshon area of the TMI and quantities derived from it (field and gradient tensor components, and the total gradient of TMI, also known as the analytic signal amplitude). The most prominent magnetic anomalies in this area are the pronounced TMI lows associated with Mount Leyshon and, to the NE of Mount Leyshon in the Mathews Pinnacle area, with two lobes of a coeval mafic dioritic intrusion, the Fenian Diorite, which carries a strong remanence of reverse polarity. Figure 2 shows profiles of the vector components along line 423400 mE, which passes through the centre of the Mount Leyshon anomaly, over the potassic alteration zone. Figures 3-4 show gradient tensor component profiles along this line and Figure 5 plots a number of rotational invariants derived from the full tensor.

The vertical component B_z is dominant within the anomaly, reflecting the subvertical down magnetisation, which produces negative poles on the upper surface of the subcropping source region, with much lower pole density on the sides of the causative body. The field vector over the source is downward pointing, producing a B_z high, and opposing the geomagnetic field, so the corresponding TMI anomaly is a low. The north component B_x is approximately antisymmetric about the centre of the source, as expected for a pole-type anomaly and the east component B_y is relatively weak. The asymmetry of the east component reflects the fact that the magnetic alteration zone is somewhat elongated SW-NE, so that the majority of the magnetised material lies west of the profile in the southern portion and east of the profile in the north.

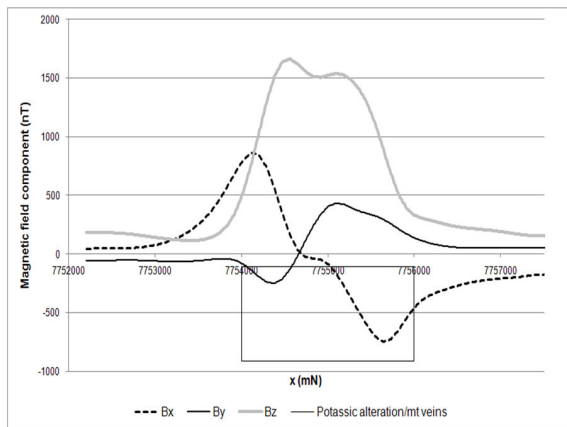


Figure 2. Magnetic vector component profiles along line 423400 mE over the Mount Leyshon anomaly, with approximate extent of the magnetic potassic alteration zone indicated. $B_{x,y,z}$ are the north, east, and down field components respectively.

Compared to the field components, the tensor element profiles show higher resolution of heterogeneity within the magnetic alteration zone, with emphasis on shallower sources. The double-humped form of the B_{zz} profile, in particular, highlights the presence of two lobes within the Mount Leyshon anomaly. The peaks in the scaled source strength profile in Figure 5 provide a good indication of the northing of these strong magnetic zones.

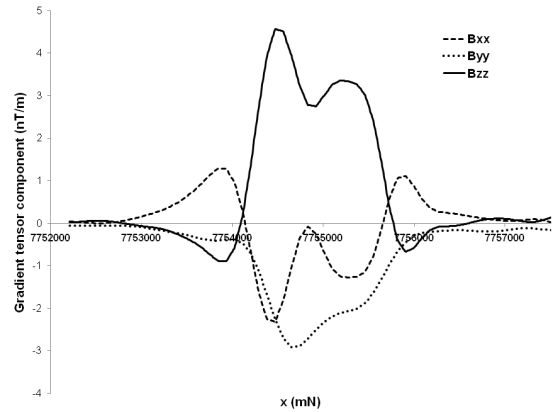


Figure 3. Diagonal elements of the calculated gradient tensor along line 423400 mE.

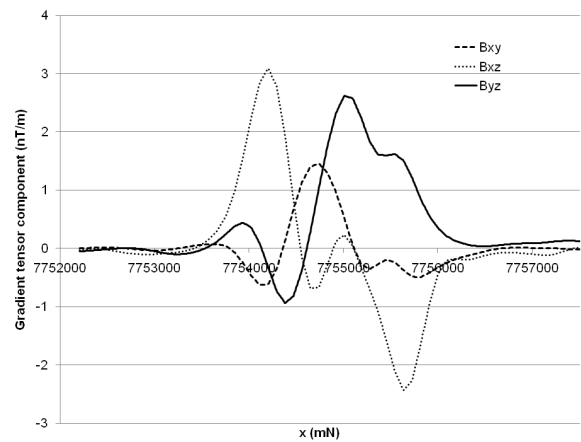


Figure 4. Off-diagonal elements of the calculated gradient tensor along line 423400 mE.

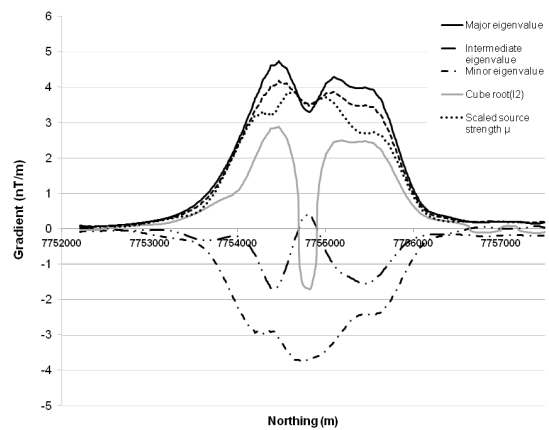


Figure 5. Rotational invariants of the calculated gradient tensor along line 423400 mE. The square root of I_1 and the cube root I_2 of have been taken so that all quantities are in the same units (nT/m) as the gradient tensor elements.

The source region of the Mount Leyshon anomaly evidently does not conform closely to either a point pole or a sphere (point dipole) model for this data set, but it is nevertheless of interest to apply simple methods of analysis developed for these models, to test their robustness in less-than-ideal conditions. Simple models should, in fact, work better on magnetic data that has been continued upward to a level where the source zone can be considered compact, at least in lateral extent.

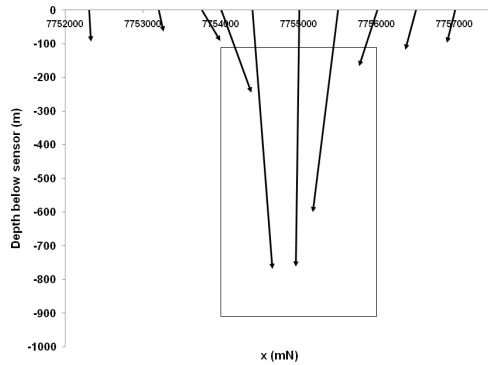


Figure 6. Projected magnetic field vectors along line 423400 mE, indicating directions to pole-type sources at the top of a reversely magnetised magnetic zone. The putative extent in cross-section of the potassic alteration zone is indicated by the box. The bottom of the zone has not been delineated by drilling.

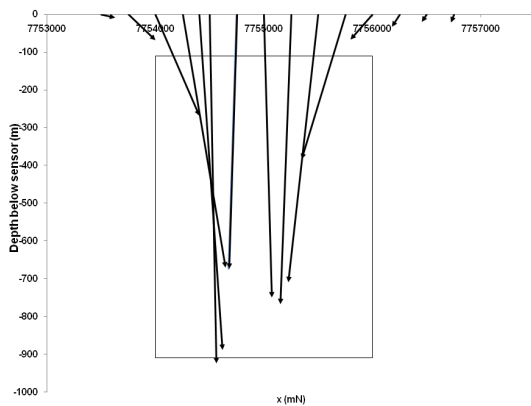


Figure 7. Projected major eigenvectors of the gradient tensor along line 423400 mE.

Along line 42300 mE the anomalous field vectors lie almost in the N-S vertical plane. Figure 6 shows projections of these vectors onto the vertical plane containing the profile. For a narrow vertical pipe, of great depth extent, with steep downward magnetisation, the extensions of the field vectors should converge on the top of the pipe, which acts as a point south pole. The lateral extent of the magnetic source zone produces subparallel, near-vertical vectors over the central portion of the anomaly, as expected. However the steepness of the vectors either side of the source zone, which results in convergence well below the mapped top of the magnetic zone, indicates a “centre of pole density” that appears to lie well below the surface. This suggests that the magnetisation may be larger at depth than near the surface. Figure 7 shows the

corresponding projections of major eigenvectors of the tensor, which should also point directly towards a pole-type source. The pattern is similar to that of Figure 6, lending support to the applicability of a pole-type model, and to the interpretation given above.

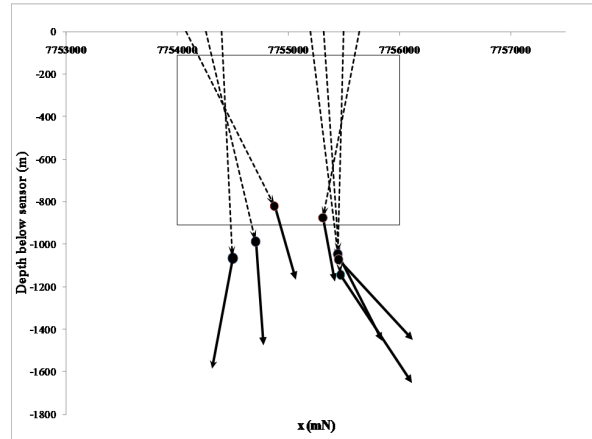


Figure 8. Locations of equivalent dipoles, inverted from anomalous field vectors and gradient tensors, shown as dots terminating inferred displacement vectors from measurement locations (dashed arrows). Solid arrows indicate projected magnetic moment vectors corresponding to each solution.

The method of Nara *et al.* (2006) was applied to vector and tensor data over the main anomalous zone along line 423400 mE. Figure 8 plots the solutions obtained for the location of the “centres of magnetisation”, assuming a dipole source, and the corresponding magnetic moment.

The average location for the three southernmost solutions is 423360 mE, 7754700 mN, depth below sensor (surface) 960 m (880 m), and for solutions from the four northernmost stations is 423820 mE, 7755420 mE, depth below sensor (surface) 1040 m (960 m). The corresponding inferred magnetic moments are 9.1×10^9 Am² (dec = 82°, inc = +81°) and 1.3×10^{10} Am² (dec = 55°, inc = +37°) for the southern and northern solution clusters respectively.

These clusters of solutions correspond to the two main lobes of the Mount Leyshon anomaly, with the southern lobe centred just west of the line and the northern lobe centred about 400 m east of the the line, consistent with the patterns exhibited by the full anomaly grid. This illustrates the power of full vector and tensor measurements along widely spaced lines, as sources that lie to one side of the lines can be defined. If we take the dipole solutions at face value, the depth estimates put the equivalent centre of depth-integrated magnetisation about 900 m below the surface, suggesting a total vertical extent of about 1800 m for the magnetic zone.

The resultant magnetisation direction at Mount Leyshon represents competition between a dominant south and steep down remanence and induced magnetisation, directed just east of north with moderate upward inclination. The inverted magnetic moments suggest that remanence is strongly dominant in the southern lobe, and less dominant over induction in the northern lobe. The overall magnetic moment of the magnetic zone appears to be about 10^{10} Am². A

magnetic zone with dimensions of $1.5 \text{ km} \times 1.5 \text{ km} \times 2 \text{ km}$ (vertical) has a volume of $4.5 \times 10^9 \text{ m}^3$, which requires an average magnetisation of about 2 A/m to account for the moment. Reducing the available volume to $1 \times 1 \times 2 \text{ km}^3$ increases the required magnetisation to 5 A/m .

Such magnetisations are well within the range of measured magnetic properties for the potassic zone at Mount Leyshon (Sexton *et al.*, 1995; Clark and Lackie, 2003). The AMIRA P700 database (Clark *et al.*, 2004) gives average remanent intensities of 7.5 A/m (SI susceptibility $k = 0.06$, Koenigsberger ratio $Q = 3.1$) for biotite-magnetite altered dolerite and 4.2 A/m ($k = 0.048 \text{ SI}$, $Q = 2.2$) for biotite-magnetite altered Puddler Creek Formation. Resultant magnetisations in this case are approximately given by the remanence intensity multiplied by $(1-1/Q)$, as the induced magnetisation is roughly antiparallel to the remanence.

To supplement the analysis of line 423400 mE, which passes directly over the anomaly, data from line 422500 mE, which passes to the west of the main anomaly, were also analysed. Figures 9 and 10 show, respectively, field vectors and major eigenvectors in plan view. The vectors shown all have shallow plunges to the east and converge at moderate depths within the magnetic source region. This again illustrates the ability of vector and tensor data to aid interpretation of off-line sources. The data hint at an extension of the magnetic zone at depth to the north, passing beneath the Mount Leyshon pit, although some of the signature could result from a negative magnetisation contrast between the nonmagnetic porphyries and mineralised breccias of the mine area, which have been strongly overprinted by magnetite-destructive phyllic alteration, and the slightly magnetic Fenian Granite host rock.

CONCLUSIONS

Eigenvector analysis and other methods for interpretation of magnetic gradient tensor data, some of which are outlined in this paper, provide powerful tools for exploiting the extra information provided by gradient tensor surveys. In the absence of gradient tensor measurements, Fourier processing of TMI data of sufficiently high quality can, in suitable circumstances, yield useful calculated estimates of anomalous magnetic field vectors and gradient tensors. The methods that are being developed for vector and gradient tensor data are equally applicable to calculated data.

Preliminary analysis of calculated vector and tensor data over Mount Leyshon has demonstrated the utility of these data types for locating sources and defining magnetisations, even when the source does not match the assumed models perfectly.

ACKNOWLEDGMENTS

I thank Clive Foss for providing grids of the field and tensor components over the Mount Leyshon area. This work comprises part of a Ph.D. project in the Department of Earth and Planetary Sciences at Macquarie University, under the supervision of Dr Mark Lackie.

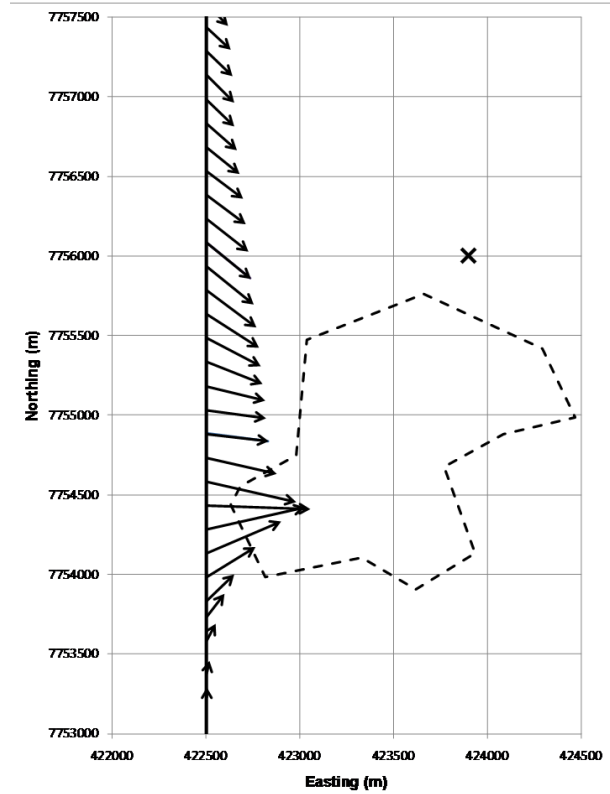


Figure 9. Plan view of magnetic field vectors along line 422500 mE. The potassic alteration zone is indicated by the dashed outline. The cross indicates the Mount Leyshon mine.

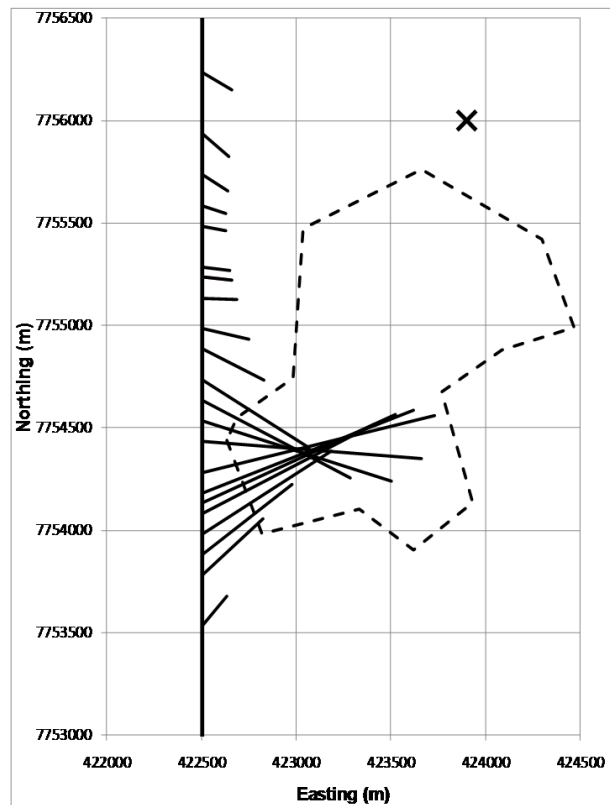


Figure 10. As for Figure 9, showing major eigenvectors.

REFERENCES

- Anton, H. and Torres, C., 2000, *Elementary Linear Algebra: Applications Version*, Eighth Edition, Wiley, New York.
- Beiki, M., Pedersen, L.B. and Nazi, H., 2011, Interpretation of aeromagnetic data using eigenvector analysis of pseudogravity gradient tensor, *Geophysics*, 76, L1, doi:10.1190/1.3555343.
- Blakely, R.J., 1996, *Potential Theory in Gravity and Magnetic Applications*, Cambridge University Press.
- Bracken, R.E. and Brown, P.J., 2006, Concepts and Procedures Required for Successful Reduction of Tensor Magnetic Gradiometer Data Obtained from an Unexploded Ordnance Detection Demonstration at Yuma Proving Grounds, Arizona, US Geological Survey Open-File Report 2006-1027.
- Christensen, A. and Rajagopalan, Shanti, 2000, The magnetic vector and gradient tensor in mineral and oil exploration, *Preview*, 84, p.77.
- Chwala, A., Stolz, R., IJsselsteijn, R., Schultze, V., Ukhansky, N., Meyer, H.-G. and Schüller, T., 2001, SQUID gradiometers for archaeometry, *Superconductor Science and Technology*, 14, 1111–1114.
- Clark, D.A., Schmidt, P.W., Coward, D.A. and Huddleston, M.P., 1998, Remote determination of magnetic properties and improved drill targeting of magnetic anomaly sources by Differential Vector Magnetometry (DVM), *Exploration Geophysics*, 29, 312-319.
- Clark, D.A. and Lackie, M.A., 2003, Palaeomagnetism of the Early Permian Mount Leyshon Intrusive Complex and Tuckers Igneous Complex, North Queensland, Australia, *Geophysical Journal International*, 153, 523-547.
- Clark, D.A., Geuna, S. And Schmidt, P.W., 2004, Predictive magnetic exploration models for porphyry, epithermal and iron oxide copper-gold deposits: implications for exploration. AMIRA P700 Final Report, CD ROM.
- Clark, D.A., Young, J.A. and Schmidt, P.W., 2009, Magnetic Tensor Gradiometry in the Marine Environment: Correction of Electric And Magnetic Field And Gradient Measurements in a Conductive Medium and Improved Methods for Magnetic Target Location Using the Magnetic Gradient Tensor, MARELEC (Marine Electromagnetics) Conference, Stockholm, July, 2009, 10pp. CD-ROM.
- Clark, D.A., 2010, Method and apparatus for detection using magnetic gradient tensor. U.S. Patent Application Pub. No.: US 2010/0211337 A1, Pub. Date: Aug. 19, 2010.
- Clem, T.R., Froelich, M.C., Overway, D.J., Purpura, J.W., Wiegert, R.F., Koch, R.H., Lathrop, D.K., Rozen, J., Eraker, J.H., Schmidt, J.M., 1997, Advances in sensor development and demonstration of superconducting gradiometers for mobile operation, *IEEE Transactions on Applied Superconductivity*, 7, 3287-3293.
- Clem, T.R., Overway, D.J., Purpura, J.W., Bono, J.T., Koch, R.H., Rozen, J., Keeefe, G.A., Willen, S. and Mohling, R.A., 2001, High-Tc SQUID gradiometer for mobile magnetic anomaly detection, *IEEE Transactions on Applied Superconductivity*, 11, 871-875.
- Fitzgerald, D. and Holstein, H., 2006, Innovative data processing methods for gradient airborne geophysical data sets. *The Leading Edge*, 25(1), 87-94.
- Fitzgerald, D., Argast, D., Paterson, R. and Holstein, H., 2009, Full tensor magnetic gradiometry processing and interpretation developments, 11th SAGA Technical Meeting and Exhibition, Swaziland, 16-18 September, 2009, 265-272.
- Fitzgerald, D., Argast, D., Paterson, R. and Holstein, H., 2010, Progress on interpreting dykes from full tensor magnetic gradiometry, *SEG Expanded Abstracts*, 29, 1162, doi:10.1190/1.3513050
- Flury, S. And Munsch, M., 2010, Review of magnetic functions for geophysical prospecting, Abstract #NS23A-1441, AGU Fall Meeting, San Francisco, 2010.
- Foss, C., 2006, The improvements in source resolution that can be expected from inversion of magnetic field tensor data, *The Leading Edge*, 25(1), 81-84.
- Heath, P., 2007, *Analysis of potential field gradient data: forward modelling, inversion and near-surface exploration*, Ph.D. thesis, University of Adelaide.
- Holstein, H., Fitzgerald, D., Willis, C.P. and Foss, C., 2011, Magnetic gradient tensor eigen-analysis for dyke location, 73rd EAEG Conference and Exhibition, Vienna, May 23-27, 2011, Vienna.
- Humphrey, K.P., Horton, T.J. and Keene, M.N., 2005, Detection of mobile targets from a moving platform using an actively shielded, adaptively balanced SQUID gradiometer, *IEEE Transactions on Applied Superconductivity*, 15 (2), 753-756.
- Ku, C.C. and Sharp, J.A., 1983, Werner deconvolution for automated magnetic interpretation and its refinement using Marquardt's inverse modeling, *Geophysics*, 48, 754-774.
- Leslie, K.E., Bick, M., Binks, R.A., Tilbrook, D.L., Clark, D.A., Schmidt, P.W., Cusack, P.J., Thorn, R.G., Blay, K. R. And Sullivan, P.R., 2005, Performance issues for a spinning gradiometer, 10th International Superconductive Electronics Conference (ISEC 2005); Noordwijkerhout, The Netherlands. 2005: OO-01.
- Leslie, K.E., Blay, K., Clark, D., Schmidt, P., Tilbrook, D., Bick, M. and Foley, C., 2007, Helicopter trial of magnetic tensor gradiometer. ASEG 19th International Conference, December 2007, Perth, Western Australia, 4 pp., CD ROM.
- Lima, E.A., Irimia, A. and Wikswo, J.P., 2006, The magnetic inverse problem, *In* J. Clarke and A.I. Braginski (Eds.), *The SQUID Handbook*, Vol. II Applications of SQUIDs and SQUID Systems, Wiley-VCH, Weinheim, pp.139-267.

- McRae, W., Veryaskin, A.V., Greager, D., Ju, L., Blair, D., Chin, E-J, Dumas, J-C and Lee, B., 2004, String magnetic gradiometer system: recent airborne trials, Society of Exploration Geophysicists 74th Annual Meeting, Expanded Abstracts 23, 790-793.
- Nara, T., Suzuki, S., and Ando, S., 2006, A Closed-Form Formula for Magnetic Dipole Localization by Measurement of Its Magnetic Field and Spatial Gradients, IEEE Transactions on Magnetism, 42, 3291-3293.
- Pedersen, L.B. and Rasmussen, T.M., 1990, The gradient tensor of potential field anomalies: Some implications on data collection and data processing of maps, Geophysics, 55, 1558-1566.
- Reid, A.B., 1980, Aeromagnetic Survey Design, Geophysics, 45, 973-976.
- Schmidt, P.W., 2006, Inversion using Euler deconvolution of the magnetic gradient tensor, Australian Earth Sciences Congress, Melbourne, Extended Abstracts, 3pp.
- Schmidt, P., Clark, D., Leslie, K., Bick, M., Tilbrook, D. and Foley, C., 2004, GETMAG – A SQUID magnetic tensor gradiometer for mineral and oil exploration, Exploration Geophysics, 35, 297-305.
- Schmidt, P.W. and Clark, D.A., 2006, The magnetic gradient tensor: Its properties and uses in source characterization, The Leading Edge, 25(1), 75-78.
- Sexton, M.A., Morrison, G.W., Orr, T.O.H., Foley, A.M. and Wormald, P.J., 1995, The Mount Leyshon magnetic anomaly, Exploration Geophysics, 26, 84-91.
- Stolz, R., L. Fritsch, and H.-G. Meyer, 1999, LTS SQUID sensor with a new configuration, Superconductor Science and Technology, 12, 806.
- Stolz, R., Zakosarenko, V., Schulz, M., Chwala, A., Fritsch, L., Meyer, H.-G. and Köstlin, E. O., 2006a, Magnetic full-tensor SQUID gradiometer system for geophysical applications, The Leading Edge, 25 (2), 178-180.
- R. Stolz, A. Chwala, V. Zakosarenko, M. Schulz, L. Fritsch, and H.-G. Meyer, 2006b, SQUID technology for geophysical exploration. SEG Expanded Abstracts 25, 894-898; DOI:10.1190/1.2370400.
- Sunderland, A., Golden, H., McRae, W., Veryaskin, A., Ju, L. and Blair, D., 2009, Results from a novel direct magnetic gradiometer, Exploration Geophysics, 40, 222-226.
- Tilbrook, D.L., 2004, The design of a new concept HTSC axial gradiometer, Physica C, 407, 1-9.
- Tilbrook, D.L., Clark, D.A. and Blay, K.R., 2006, Data Extraction and Calibration of a Superconducting Rotating Magnetic Tensor Gradiometer, Applied Superconductivity Conference, Seattle, August 27 – September 1, 2006.
- Veryaskin, A.V., 2001, Magnetic gradiometry: a new method for magnetic gradient measurement, Sensors and Actuators A, 91, 233-235.
- Wiegert, R., Oeschger, J., and Tuovila, E., 2007, Demonstration of a novel man-portable magnetic STAR technology for real time localization of unexploded ordnance, Proceedings of MTS/IEEE Oceans 2007, DOI 10.1109/OCEANS.2007.4449229.
- Wilson, H., 1985. Analysis of the Magnetic Gradient Tensor. Defence Research Establishment Pacific, Canada, Technical Memorandum, 85-13, 47.
- Wynn, W.M., Frahm, C.P., Carroll, P.J., Clark, R.H., Wellhoner, J. and M.J. Wynn, 1975, Advanced superconducting gradiometer/magnetometer arrays and a novel signal processing technique, IEEE Trans. Magn., MAG-11, 701-707.
- Wynn, W.M., 1995, Magnetic dipole localization using the gradient rate tensor measured by a five-axis magnetic gradiometer with known velocity, Proc. SPIE, 2496, 357-367.
- Wynn, W.M., 1997, Magnetic dipole localization with a gradiometer: obtaining unique solutions, IGARSS '97. Remote Sensing – A Scientific Vision for Sustainable Development, Geoscience and Remote Sensing, IEEE International, Vol. 4, 1483-1485.
- Wynn, W.M., 1999, Detection, localization, and characterization of static magnetic-dipole sources, In C.E. Baum (Ed.), Detection and Identification of Visually Obscured Targets, Taylor & Francis, Philadelphia, pp. 337-374.
- Young, J.A., S.T. Keenan, D.A. Clark, K.E. Leslie, P. Sullivan, P. Fairman, C. Williams, C.P. Foley and S.D. Billings, 2010, A Superconducting Magnetic Tensor Gradiometer for Underwater UXO Detection. 21st International Geophysical Conference & Exhibition (ASEG-PESA 2010); Sydney [extended abstract]. 4 pp. CD ROM.

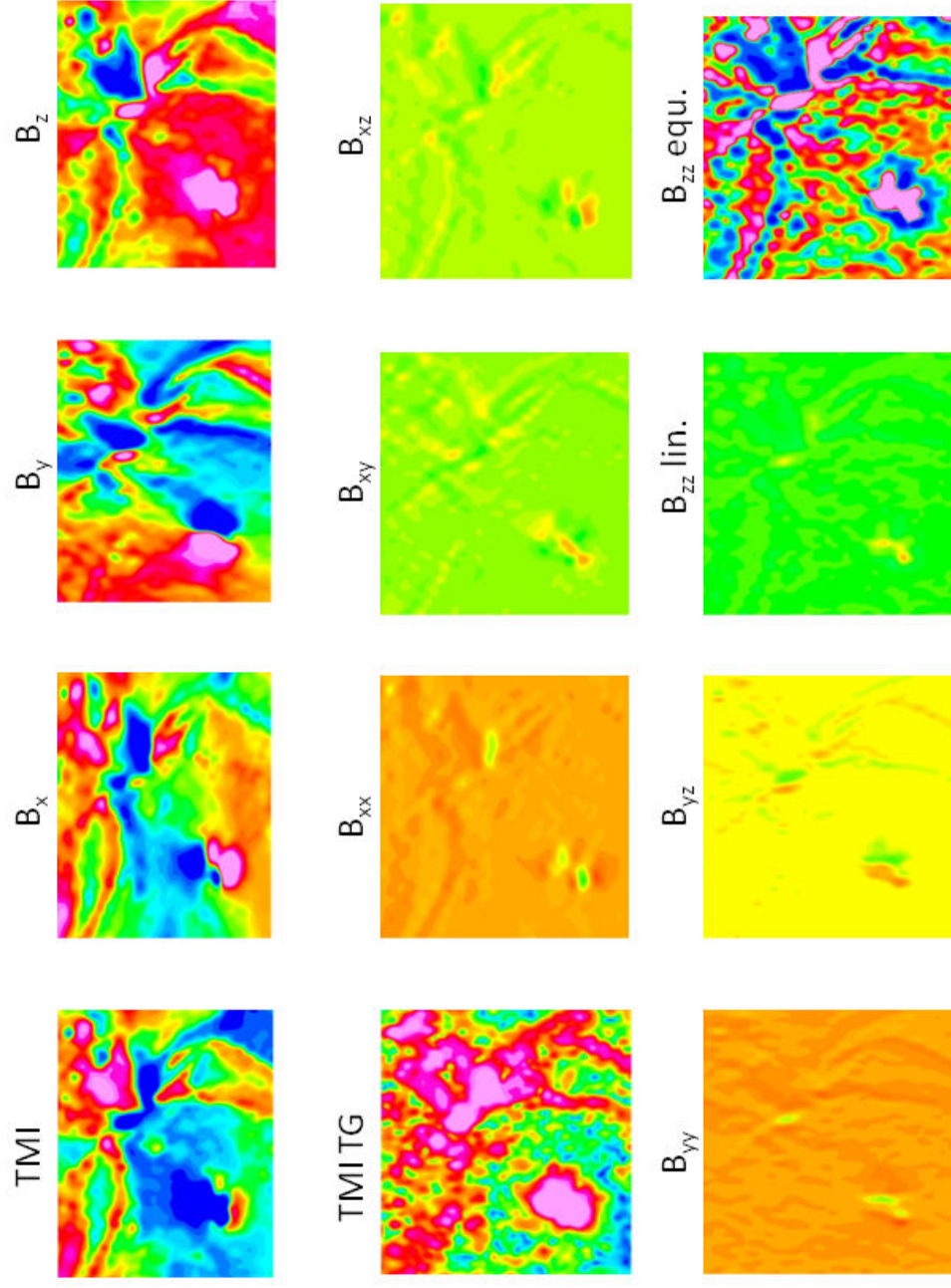


Figure 1. Magnetic anomalies over the Mount Leyshon – Mathews Pinnacle area. TMI = total magnetic intensity, B_x = calculated N component, B_y = calculated E component, B_z = calculated down component, TMITG = total gradient (analytic signal amplitude) of TMI, B_{ij} = calculated gradient tensor elements, e.g. B_{xz} lin. = calculated downward derivative of down component (linear stretch). All field components images have a histogram equalised stretch, all tensor element images have a linear stretch, except for B_z equ., which has a histogram equalised stretch. The Mount Leyshon anomaly is the prominent TMI low/vertical component high in the SW of the image. The prominent TMI lows in the NE quadrant of the image are associated with two outcropping lobes of the Fenian Diorite, which wrap around the SW side of the TMI high associated with Devonian granodiorite intrusions.